

CHARACTERISTIC MASSES IN GALAXY QUENCHING: ENVIRONMENTAL VERSUS INTERNAL EFFECTS

PENGFEI LI^{1,2}, HUIYUAN WANG^{1,2}, H.J. MO³, ENCI WANG⁵, HUI HONG^{1,2}*Draft version March 27, 2020*

ABSTRACT

A clear transition of galaxy quenching is identified in the multi-parameter space of stellar mass (M_*), bulge to total mass ratio (B/T_m), halo mass (M_h) and halo-centric distance (r/r_{180}). For a given halo mass, the characteristic stellar mass ($M_{*,c}$) for the transition is about one-fifth of the stellar mass of the corresponding central galaxy, and almost independent of B/T_m . Once B/T_m is fixed, the quenched fraction of galaxies with $M_* < M_{*,c}$ increases with M_h , but decreases with M_* in the inner part of halos ($r/r_{180} < 0.5$). In the outer part ($r/r_{180} > 0.5$), the trend with M_h remains but the correlation with M_* is absent or becomes positive. For galaxies above $M_{*,c}$ and with B/T_m fixed, the quenched fraction increases with M_* , but depends only weakly on M_h in both the inner and outer regions. In general the quenched fraction increases with B/T_m when other parameters are fixed. We discuss the implications of the characteristic stellar mass for internal and environmental quenching processes. Our results suggest that environmental quenching is important only for galaxies with $M_* < M_{*,c}$, while internal quenching plays the dominating role for high-mass galaxies. The efficiencies of internal and environmental quenching both depend on B/T_m .

Subject headings: galaxies: halos - galaxies: general – methods: observational - methods: statistical

1. INTRODUCTION

In the local Universe, galaxies can be divided into two populations according to their star formation activity or rest-frame color (e.g. [Strateva et al. 2001](#); [Brinchmann et al. 2004](#); [Wetzel et al. 2012](#)). One population lies in the star forming main sequence, where galaxies in general have blue color and disk-like morphology, and the other is the passive or quenched population, in which galaxies have red color, spheroid-like morphology, and little on-going star formation. The quenched population is observed to be present at redshift as high as $z = 1$ (e.g. [Bell et al. 2004](#); [Ilbert et al. 2013](#); [Tomczak et al. 2014](#)), and continuously grows with time, indicating that the quenching process drives the evolution of the galaxy population over most of the Hubble time.

Many mechanisms have been proposed for the quenching of star formation. In broad terms, the quenching processes are divided into two categories. The first is internal, such as supernova feedback (e.g. [White & Rees 1978](#); [Murray et al. 2011](#)) and active galactic nuclei (AGN) feedback (e.g. [Croton et al. 2006](#); [Heckman & Best 2014](#)), which may disperse inter-stellar media (ISM) or prevent gas from cooling so as to reduce the cold gas reservoir for star formation, and morphological quenching (e.g. [Martig et al. 2009](#)), in which cold gas disk is made stable by a massive bulge. The strengths of these mechanisms are expected to depend on galaxy stellar mass (or bulge mass) and structural properties, so

that the fraction of the quenched galaxies (quenched fraction) is expected to be correlated with the stellar mass, bulge mass, and the bulge to total ratio (hereafter B/T) of galaxies. This may be why massive, bulge-dominated early type galaxies are usually observed to have low on-going star formation activities. But the explanation of these correlations is not yet conclusive ([Lilly & Carollo 2016](#)).

The second category is environmental processes. These include ram pressure stripping (e.g. [Gunn & Gott 1972](#); [Abadi et al. 1999](#)) and tidal stripping (e.g. [Toomre & Toomre 1972](#); [Read et al. 2006](#)), which remove the ISM from galaxies, and strangulation (e.g. [Larson et al. 1980](#); [Balogh et al. 2000](#)), a process that cuts off the replenishment of star forming gas. Interaction and merger of a galaxy with other galaxies, which can consume or disperse cold gas by triggering star formation and/or AGN activity (e.g. [Moore et al. 1996](#); [Di Matteo et al. 2005](#)), are two other processes in this category. These environmental processes are expected to produce a quenched fraction that depends on environment, such as the mass of the halo that hosts the galaxy, and the distance of a galaxy from the center of its host halo (halo-centric distance). Moreover, since lower-mass galaxies generally have shallower local gravitational potential wells and are more prone to environmental effects, the trend of the quenching with galaxy stellar mass produced by environmental processes is expected to be the opposite to that produced by internal processes.

With the advent of large photometric and spectroscopic surveys of galaxies, the star formation properties of galaxies, and their correlations with both internal properties and environment, have been investigated extensively (e.g. [Baldry et al. 2006](#); [Weinmann et al. 2006](#); [van den Bosch et al. 2008](#); [Peng et al. 2010](#); [Wetzel et al. 2012](#); [Woo et al. 2013](#); [Bluck et al. 2014](#); [Teimoorinia et al. 2016](#); [Liu et al. 2019](#)). For example, the investigations of [Peng et al. \(2010\)](#) and [Liu et al.](#)

¹ Key Laboratory for Research in Galaxies and Cosmology, Department of Astronomy, University of Science and Technology of China, Hefei, Anhui 230026, China; lpfv@mail.ustc.edu.cn, whywang@ustc.edu.cn

² School of Astronomy and Space Science, University of Science and Technology of China, Hefei 230026, China

³ Department of Astronomy, University of Massachusetts, Amherst MA 01003-9305, USA

⁵ Department of Physics, ETH Zurich, Wolfgang-Pauli-Strasse 27, CH-8093 Zurich, Switzerland

(2019) suggest that the quenching of massive galaxies may be dominated by internal processes, while environmental processes play a more important role in less massive galaxies. When considering the roles of dark matter halos on galaxy quenching, it is generally believed that the quenching of central galaxies in halos are dominated by internal processes, while halo-specific environment plays important roles only for satellite galaxies (e.g. van den Bosch et al. 2008). However, this simple central-satellite dichotomy has been found to be insufficient to account for quenching in the observed galaxy population. Indeed, several studies have found that satellites and centrals are quite similar in their star formation activity, AGN prevalence, morphology and sizes when stellar mass and environment are properly controlled (e.g. Hirschmann et al. 2014; Knobel et al. 2015; Bluck et al. 2016; Wang et al. 2018b,a, 2020), although there have also been investigations that found the opposite (e.g. Davies et al. 2019).

Wang et al. (2018b,a, 2020) further found that galaxies above and below one-fifth of the central galaxy stellar mass exhibit different dependence of the quenched fraction, B/T and size on the halo-centric distance. Based on the relation between central mass and halo mass relation proposed in Yang et al. (2009), Wang et al. (2020) proposed a characteristic stellar mass,

$$M_{*,c} = \frac{M_0}{5} \frac{(M_h/M_1)^{\alpha+\beta}}{(1 + M_h/M_1)^\beta} \quad (1)$$

where $\log_{10}(M_0/M_\odot) = 10.31$, $\log_{10}(M_1/M_\odot) = 11.04$, $\alpha = 0.31$, and $\beta = 4.54$. This implies that galaxies above and below this demarcation mass may be affected by the halo environment differently.

Despite of all the progress, there are still large uncertainties as to which processes are physically responsible for the quenching of galaxies. One of the most important reasons is that the observed correlations are usually the results of several processes, which cannot be easily disentangled. In this paper, we perform a detailed analysis about the significance of the characteristic stellar mass that can potentially separate environmental and internal effects. We consider the galaxy population as a whole, rather than investigating centrals and satellites separately. In particular, we include galaxy morphology as an important parameter in our analysis.

The paper is organized as follows. Section 2 presents galaxy and group catalogs we use, as well as physical quantities we derive from them. In Section 3, we investigate how the quenched population is correlated with various parameters that quantify internal and external effects, focusing on the presence of characteristic stellar mass scales in the quenching population. Finally, we summarize our results in Section 4.

2. OBSERVATIONAL DATA

Our galaxy sample is taken from the New York University Value Added Galaxy Catalog (NYU-VAGC; Blanton et al. 2005), which is based on the Sloan Digital Sky Survey (SDSS) DR7 (Abazajian et al. 2009). Following the construction of the group catalog, we select galaxies in the redshift range $z = 0.01$ - 0.2 , with spectroscopic completeness (C) larger than 0.7 and with the r -band magnitude limit of 17.72 mag. Among these galaxies,

a total of 32,348 galaxies (about 6%) that do not have estimates of star formation rate or bulge-to-total ratio (B/T) are discarded. Our final sample contains 511,728 galaxies.

Stellar masses of individual galaxies, M_* (in unit of $h^{-2}M_\odot$), are obtained by using the relation between the $(g-r)$ color and the stellar mass-to-light ratio as given by Bell et al. (2003) assuming a Kroupa & Weidner (2003) initial mass function (IMF). Star formation rates (SFRs) of the galaxies are adopted from the MPA-JHU catalog⁵. They are estimated from the SDSS spectra using an updated version of the method presented in Brinchmann et al. (2004) and a Kroupa IMF. We separate galaxies into a star-forming population and a quenched population using the demarcation line proposed by Bluck et al. (2016).

We use the bulge to total mass ratio (B/T_m) of a galaxy as an indicator of its morphological type. Extending the work of Simard et al. (2011), Mendel et al. (2014) obtained the bulge+disk decomposition for SDSS images in the u , g , r , i , and z bands. They then estimated the bulge and disk stellar masses by modeling the corresponding broadband spectral energy distribution. We adopt the ratios between the bulge mass and the bulge+disk mass given in Mendel et al. (2014) as the B/T_m for our sample galaxies. We have also tested our results with r -band bulge to total light ratio from Simard et al. (2011), which does not change our conclusions.

The group catalog used here is constructed by using the halo-based group finder of Yang et al. (2007). The host halo mass (M_h) of each group is estimated using a abundance matching method based on the total stellar mass of all member galaxies brighter than $M_r = -19.5 + 5 \log h$ in the r -band. The most massive galaxy in a group is defined as the central galaxy of the group while all the rest (if any) as satellite galaxies. For each member galaxy in a group, we define a halo-centric distance, r/r_{180} , where r is the projected distance between the galaxy and the luminosity-weighted center of the group. The halo virial radius, r_{180} , is estimated using equation (5) in Yang et al. (2007).

The statistical quantity investigated here is the quenched fraction, which is defined as the fraction of galaxies that are quenched according to the criterion described above. For a given sub-sample of N galaxies, the quenched fraction, f_Q , is calculated as:

$$f_Q = \frac{\sum_{i=1}^N \omega_i q_i}{\sum_{i=1}^N \omega_i}, \quad (2)$$

where q_i is the quenching property for the i th galaxy and ω_i is a weight assigned to the galaxy. If a galaxy is quenched, $q_i = 1$, otherwise $q_i = 0$. The weight is defined as $\omega = 1/(V_{\max}C)$. Here V_{\max} , calculated using the K -correction utilities, v4.2, of Blanton & Roweis (2007), is used to correct for the Malmquist bias, and C is the redshift incompleteness obtained from the NYU-VAGC.

3. THE QUENCHED POPULATION AND CHARACTERISTIC STELLAR MASS

The left panel of Figure 1 shows the quenched fraction, f_Q , as a function of M_h and M_* , sampled on

⁵ <http://www.mpa-garching.mpg.de/SDSS/DR7/>

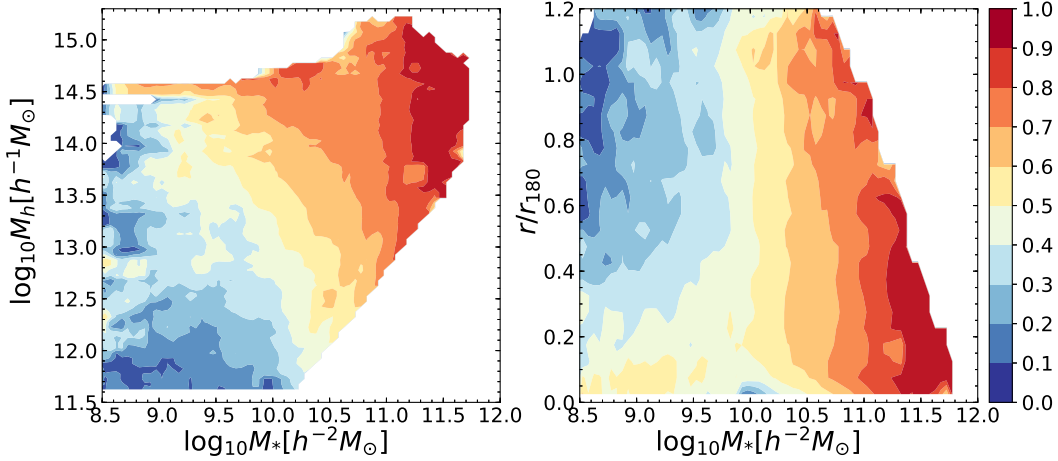


FIG. 1.— The left panel shows f_Q as a function of M_h and M_* while the right panel shows f_Q as a function of r/r_{180} and M_* . The results are smoothed on grids with a cell size given by $\Delta \log(M_h/h^{-1}M_\odot) = 0.2$, $\Delta \log(M_*/h^{-2}M_\odot) = 0.2$ and $\Delta r/r_{180} = 0.1$. See the text for the details about the smoothing procedure.

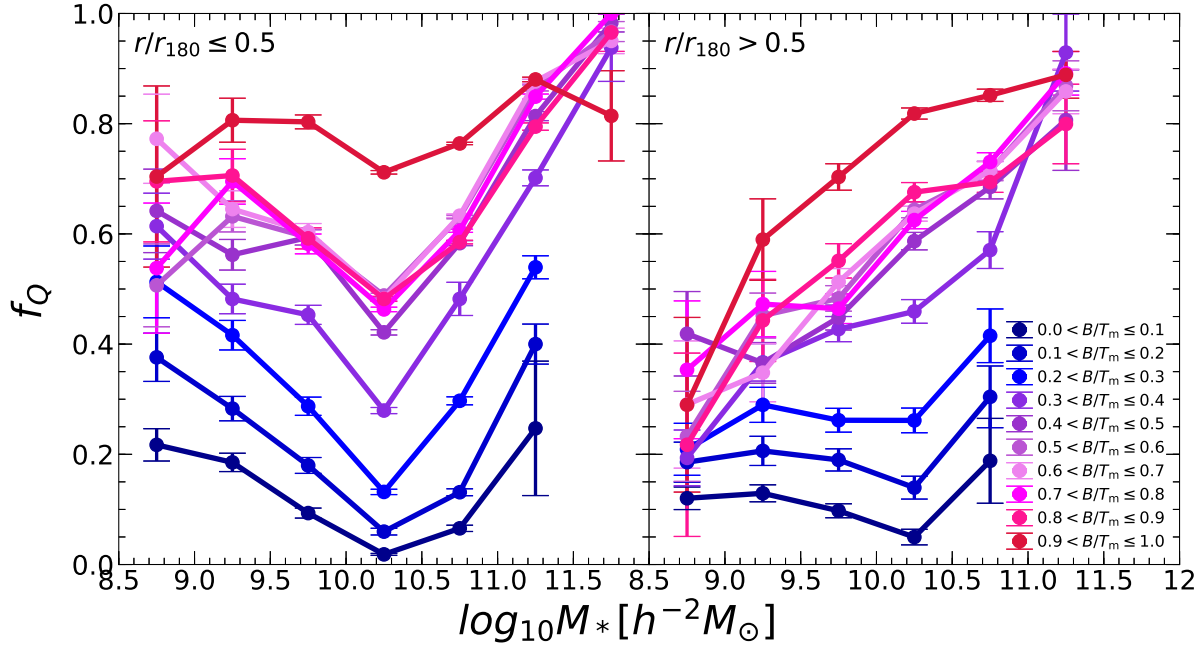


FIG. 2.— f_Q as a function of M_* . The left panel is for $r/r_{180} \leq 0.5$ while the right panel for $r/r_{180} > 0.5$. Different colors represent different B/T_m . Samples containing less than 10 galaxies are not used. Error bars are estimated by using 1,000 bootstrap samples.

a grid. The value of f_Q at each grid point is calculated using galaxies within a pixel with size given by $\Delta \log(M_h/h^{-1}M_\odot) = 0.2$ and $\Delta \log(M_*/h^{-2}M_\odot) = 0.2$. If the number of galaxies in the pixel is less than 10, the pixel and the corresponding grid point is ignored.

As one can see, f_Q increases almost monotonously with both M_* and M_h , consistent with results obtained previously (Weinmann et al. 2006; Wetzel et al. 2012; Wang et al. 2018b). Strong dependence on M_* can be seen at any given halo mass, but the dependence on the environment (halo mass) is different for galaxies of different M_* . For massive galaxies with $\log(M_*/h^{-2}M_\odot) > 11.0$, the dependence of f_Q on M_h is weak, as indicated by the almost vertical contours. In contrast, for galaxies of lower masses, a large gradient is seen in the vertical

direction, suggesting strong M_h dependence. A similar trend can be observed in the dependence of f_Q on M_* and r/r_{180} , shown in the right panel of Figure 1. The value of f_Q increases with M_* at any given r/r_{180} , while the dependence on r/r_{180} is different for galaxies of different M_* . For $\log(M_*/h^{-2}M_\odot) > 10$, the dependence on r/r_{180} is weak; for lower masses, the trend with r/r_{180} is clear, particularly for $r/r_{180} < 0.5$. Such dependence on r/r_{180} is consistent with results obtained previously (e.g. Wetzel et al. 2012; Woo et al. 2013).

It is known that, at a given stellar mass, the star formation activity of a galaxy may depend on its internal structure, such as the dominance of the bulge (morphology type). Moreover, the efficiencies of some environmental mechanisms are expected to depend on galaxy structure

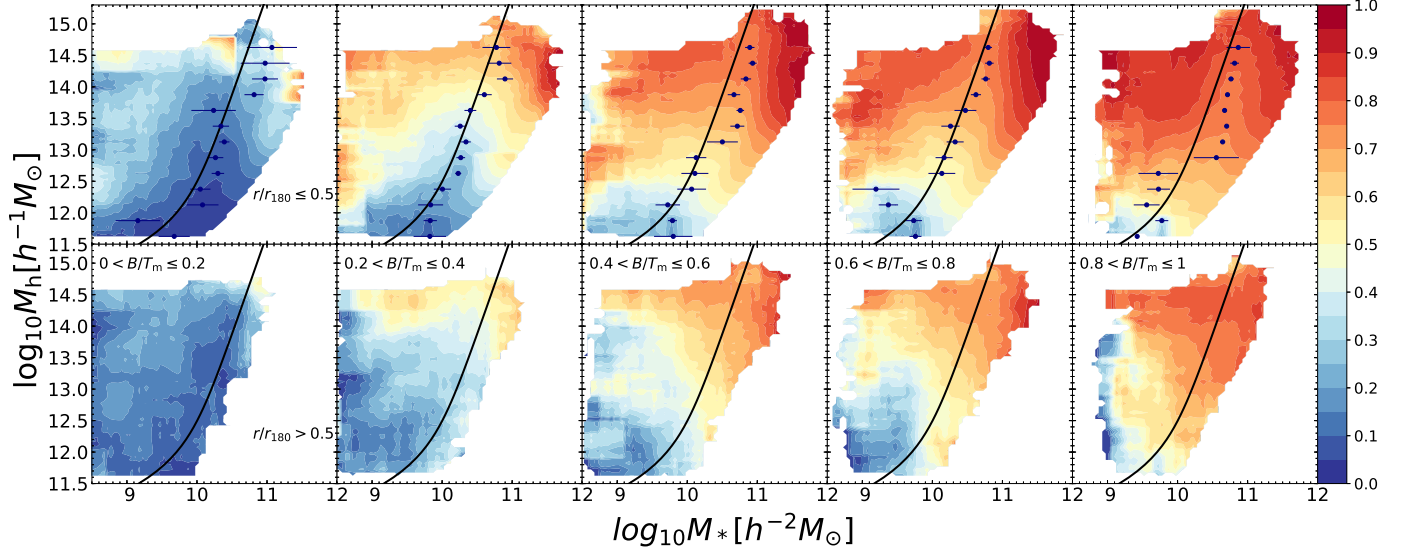


FIG. 3.— Contours show f_Q as a function of M_h and M_* . The upper panels are for galaxies with $r/r_{180} \leq 0.5$ while the lower panels are for $r/r_{180} > 0.5$. Different columns show different B/T_m , as indicated in each lower panel. The results are smoothed on a grid with cell size given by $\Delta \log(M_*/h^{-2}M_\odot) = 0.6$ and $\Delta \log(M_h/h^{-1}M_\odot) = 0.6$. The solid circles with error bars show the best-fitting $M_{*,c}$ and the black solid line shows Equation (1). See the text for details.

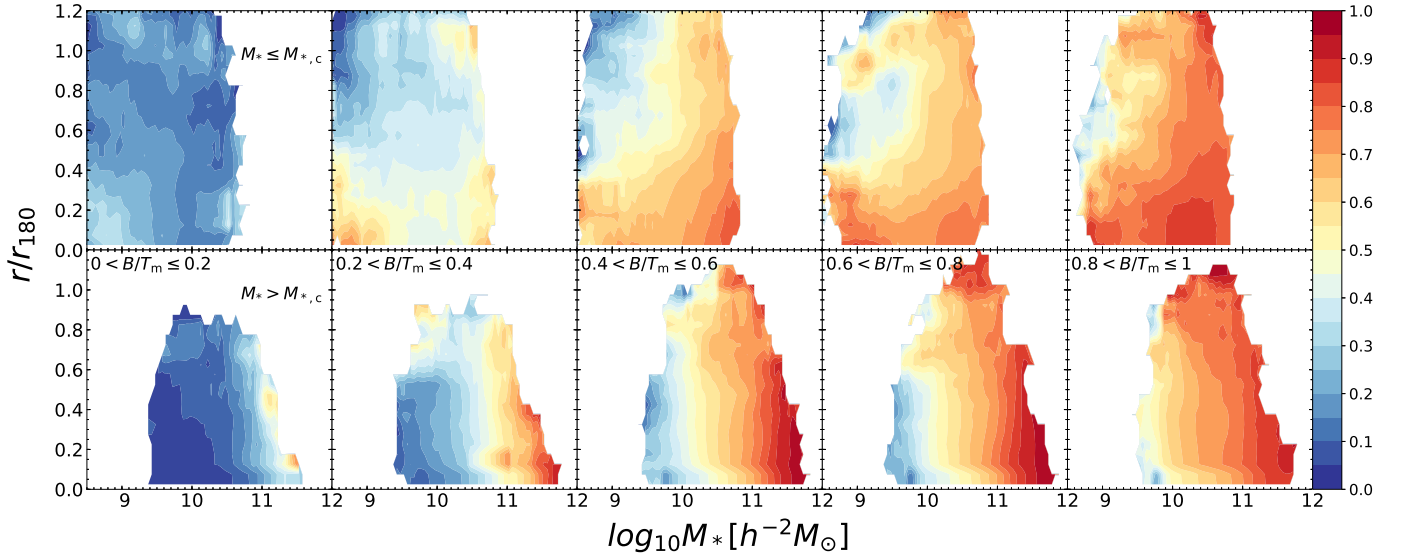


FIG. 4.— f_Q as a function of r/r_{180} and M_* . The upper panels show galaxies with $M_* < M_{*,c}$ while the lower panels show galaxies with $M_* > M_{*,c}$. Different columns show different B/T_m . The grid cell size is given by $\Delta \log(M_*/h^{-2}M_\odot) = 0.6$ and $\Delta r/r_{180} = 0.2$. See the text for the details of the smoothing procedure.

as well. At a given mass, a more extended galaxy has a shallower gravitational potential well, making it more prone to external effects. Motivated by these, we introduce B/T_m as another parameter. Figure 2 shows f_Q as a function of M_* for galaxies with different B/T_m . Since the environmental effect appears to be much stronger in the inner region, we show the results separately for $r/r_{180} < 0.5$ (left panel) and $r/r_{180} > 0.5$ (right panel).

As one can see, at any given stellar mass, f_Q increases with B/T_m in both the inner and outer regions of halos. For galaxies with $r/r_{180} < 0.5$, there is a clear transition in the M_* -dependence of f_Q : the quenched fraction first decreases with M_* at $\log(M_*/h^{-2}M_\odot) < 10.3$, and

then increases with M_* at larger masses. This behavior is observed in all B/T_m bins. In the outer region, however, f_Q depends only weakly on M_* at $B/T_m < 0.5$, but increases strongly with M_* at $B/T_m > 0.5$. The transitional feature, seen in the inner region, is noticeable but much weaker for $B/T_m < 0.5$ and is completely absent for $B/T_m > 0.5$, in the outer region. This difference between the inner and outer regions suggests that the transitional feature may be produced by the dense environment in the inner region, rather than by internal processes that are independent of environment.

Such transition is, however, absent in the total sample, as shown in the left panel of Figure 1. This owes to

the fact that galaxies of lower masses have, on average, smaller B/T_m . Thus, for the whole sample, the results for low-mass and high-mass populations are dominated, respectively, by galaxies with small and high B/T_m . The transitional feature seen for galaxies at fixed B/T_m may then be erased by the correlation between B/T_m and M_* . This suggests that galaxy morphology not only affects internal quenching, but also plays an important role in understanding environmental quenching.

Next we explore how the transitional behavior depends on host halo. Figure 3 shows f_Q as a function of M_h and M_* for different B/T_m in both inner ($r/r_{180} \leq 0.5$) and outer ($r/r_{180} > 0.5$) regions. Due to the limited number of galaxies, here we adopt a smoothing with larger pixels: $\Delta \log(M_h/h^{-1}M_\odot) = 0.6$ and $\Delta \log(M_*/h^{-2}M_\odot) = 0.6$. A valley like structure in the f_Q field across the M_h - M_* plane can clearly be seen for galaxies in the inner region and for almost all samples of B/T_m . To the left of the valley, the value of f_Q exhibits a negative correlation with M_* but a positive correlation with M_h . To the right of the valley, in contrast, f_Q shows a strong, positive correlation with M_* but weak or no dependence on M_h . The transitional feature seen in Figure 2 can also be seen here. However, the stellar mass at the transition appears to depend on M_h , as we will quantify in the following.

These results strongly suggest the existence of a characteristic stellar mass in quenching that is related to halo mass. We plot in the upper panels of Figure 3 the demarcation line (Equation 1) in the relations of galaxy size with r/r_{180} proposed by Wang et al. (2020). Remarkably, the curve lies close to the bottom of the valley-like structure. To check this quantitatively, we measure $M_{*,c}(M_h)$ directly from our data. The results in Figure 2 suggest that f_Q as a function of M_* can be approximated by a broken power law, so we use the following function to model the relation:

$$f_Q = \begin{cases} a \log M_*/M_{*,c}(M_h) + d, & (M_* < M_{*,c}) \\ b \log M_*/M_{*,c}(M_h) + d, & (M_* \geq M_{*,c}) \end{cases} \quad (3)$$

where a , b , d and $M_{*,c}$ are free parameters to be determined. The least square method is adopted to perform the fitting and the best-fitting $M_{*,c}$ is shown in Figure 3. The error bars are estimated by using 1000 bootstrap samples. Our tests with other smoothing sizes, such as $\Delta \log(M_*/h^{-2}M_\odot) = 0.4$ and 0.5 , suggest that the results are insensitive to the exact choice.

In general, the best-fitting $M_{*,c}$ can characterize the trend of the valley-like structure, suggesting that the measurement is reliable. As one can see, the measured $M_{*,c}$ - M_h relation matches Equation (1) very well, except in a small number of bins. This suggests that Equation (1) is a good approximation of $M_{*,c}$ in the $(M_h, M_*, B/T_m, r/r_{180})$ space. The fitting results also suggest that the $M_{*,c}$ - M_h relation is similar for different B/T_m . This is consistent with the results shown in Figure 2, where the averaged values of $M_{*,c}$ over different M_h are all close to $10^{10.3} h^{-2} M_\odot$ for different B/T_m . However, it is clear that $M_{*,c}$ increases with M_h . For Milky-Way size halos, $M_{*,c} \sim 10^{9.7} h^{-2} M_\odot$, while for rich clusters, $M_{*,c} \sim 10^{10.7} h^{-2} M_\odot$.

For comparison, we also show Equation (1) in the lower panels of Figure 3. Although a valley-like structure is not obvious here, galaxies to the left and right of the curve

do exhibit different behavior. For example, to the left of the curve, the correlation with M_* is weak at small B/T_m and positive at large B/T_m . To the right of the curve, on the other hand, f_Q increases with M_* much more quickly. More importantly, the M_h dependence is strong on the left side of the curve, but is weak or absent in the right. It suggests that the demarcation line can also be used to separate the environmental and internal effects for galaxies in the outer region. To further examine how $M_{*,c}$ potentially separates quenching effects, we show, in Figure 4, f_Q as a function of r/r_{180} and M_* for galaxies of different B/T_m , using $\Delta(r/r_{180}) = 0.2$ and $\Delta \log(M_*/h^{-2}M_\odot) = 0.6$. The upper and lower panels show galaxies below and above $M_{*,c}$ (Equation 1), respectively. As one can see, even at the same stellar mass, galaxies above and below $M_{*,c}$ show very different dependence on r/r_{180} . It implies that the dependence on M_h and r/r_{180} of galaxy structural and quenching properties may be produced by the same environmental mechanism (see Wang et al. 2020, for detailed discussion).

Finally, we notice that there is a kink-like structure in the contours of f_Q at the high stellar mass edge for galaxies in the inner region (upper panels of Figure 3). From the lower panels of Figure 4 one sees that this structure is produced by galaxies close to halo centers. Their high stellar mass for their halo mass and their small halo-centric distance suggest that these galaxies are dominated by centrals. Unfortunately, it is unclear if this is a real feature indicating a difference between centrals and satellites, or a false signal produced by the halo mass assignment technique based on the total stellar mass which is usually dominated by the most massive galaxies.

4. SUMMARY AND DISCUSSION

In this paper, we have investigated how galaxy quenching in star formation depends on internal properties of galaxies, as represented by their stellar mass and B/T_m , and environment, as represented by the mass of their host halos and their distances to the halo centers. Our main results can be summarized as follows.

- The quenched fraction, f_Q , depends on both internal properties and the environment of galaxies. Galaxies of higher mass and higher B/T_m have a larger f_Q ; galaxies residing in more massive halos and in the inner parts of halos are also more likely to be quenched.
- For a given B/T_m and a given host halo mass, there is a characteristic stellar mass, $M_{*,c}$, where f_Q is the lowest. The characteristic mass is about one-fifth of that of the central galaxy of the halo, almost independent of B/T_m . The presence of the characteristic mass is more prominent in the inner region of halos.
- Galaxies with masses below and above $M_{*,c}$ have different quenching properties. At $M_* < M_{*,c}$, f_Q for galaxies of a given B/T_m decreases with M_* and r/r_{180} but increases with M_h . And the dependence of f_Q on the two environmental parameters is stronger for high B/T_m galaxies than low B/T_m ones. At $M_* \geq M_{*,c}$, however, f_Q increases with M_* but is almost independent of M_h and r/r_{180} .

The trend with M_h is similar in both the inner and outer regions, but the decrease of f_Q with M_* is absent in the outer region.

These results have important implication for the understanding of quenching of galaxies. Let us first look at galaxies with $M_* > M_{*,c}$. For these galaxies f_Q depends only weakly on M_h and r/r_{180} , indicating that their quenching of star formation is dominated by internal processes. The strong increase of f_Q with both M_* and B/T_m (Figure 2 and 3) at the massive end provide support to such interpretation. It suggests that the existence of a significant bulge is essential for galaxy quenching (e.g. Bluck et al. 2014). A number of quenching mechanisms linked to galaxy bulges have been proposed. The morphological quenching, as proposed in Martig et al. (2009), is expected to predict a strong dependence of f_Q on B/T_m , consistent with what we find. However, it is unclear if the model can predict the strong M_* -dependence at fixed B/T_m seen in the data. Various types of AGN feedback models assume that the quenching of massive galaxies is made by the energy generated by the super-massive black holes whose mass is proportional to the bulge mass. These models, therefore, predict a strong positive correlation between f_Q and the bulge mass, as expected from the data. Even for low-mass galaxies where AGN feedback may not be important, star formation associated with the formation of the bulge may also suppress subsequent gas accretion and star formation in the disk (e.g. Mo & Mao 2004). Clearly, our results can be used to constrain these models once their predictions are quantified.

For galaxies with $M_* < M_{*,c}$, there is strong dependence of f_Q on both M_h and r/r_{180} even with both M_* and B/T_m controlled. This clearly indicates that quenching of these galaxies is affected by environment. Theoretically, many environmental processes, such as ram pressure and tidal stripping, predict a higher efficiency for galaxies of lower mass, because of their shallower gravitational potential wells. The decrease of f_Q with M_* at the low-mass end thus provides a strong evidence for such environmental quenching. Since some environmental mechanisms are expected to be stronger in halos of higher mass and in the inner regions of halos, the strong increase of f_Q with M_h and its decrease with r/r_{180} lend further support to our interpretation. The interpretation is not unique though, as the final environmental effect depends not only on the strength of quenching mechanisms, but also on how long these mechanisms operate. For example, Shi et al. (2020) found that satellites accreted earlier by their host halos are more frequently quenched than the counterparts accreted later. Thus, if the accretion time for a satellite depends on M_h , M_* and r/r_{180} ,

the observed correlations can be produced even if the strength of the mechanisms is independent of the three parameters. Obviously, more investigations are needed to disentangle the dependencies on accretion time and quenching strength.

As one can see from Figure 3 and 4, for $M_* < M_{*,c}$, the dependence on M_h and r/r_{180} is much stronger for high B/T_m galaxies than low B/T_m galaxies. One possibility is that feedback processes is stronger in higher B/T_m galaxies, which makes the ISM gas more fluffy and easier to strip, as shown in hydrodynamic simulations (Bahé & McCarthy 2015), so that the environmental dependence is stronger for galaxies with higher B/T_m . Another possibility is that galaxies with lower B/T_m are accreted into their hosts more recently, so that the environmental impact is smaller. Indeed, galaxies at higher redshift are expected to be more compact (Mo et al. 1999; van der Wel et al. 2014) and more likely to become a galaxies with higher B/T_m at $z = 0$. In both possibilities, environmental effects may not change the structure of a galaxy, but its star formation rate. Thus, unless B/T_m is created with strong dependence on M_h and r/r_{180} , the weak dependence of galaxy morphology on M_h and r/r_{180} (Liu et al. 2019) suggests that galaxy morphology may indeed have formed without strong dependence on environment. Our results strongly suggest that galaxy morphology, as represented by B/T_m , is an important factor in affecting the efficiency of both internal and environmental quenching processes.

ACKNOWLEDGMENTS

This work is supported by the National Key R&D Program of China (grant No. 2018YFA0404503), the National Natural Science Foundation of China (NSFC, Nos. 11733004, 11421303, 11890693, and 11522324), the National Basic Research Program of China (973 Program)(2015CB857002), and the Fundamental Research Funds for the Central Universities. P.F.L. is supported by the Fund for Fostering Talents in Basic Science of the National Natural Science Foundation of China NO.J1310021. EW is supported by the Swiss National Science Foundation. The work is also supported by the Supercomputer Center of University of Science and Technology of China. This research utilized: NumPy (van der Walt et al. 2011), a fundamental package for scientific computing with Python; SciPy (Jones et al. 2001–), a Python based ecosystem of open software for mathematics, science and engineering; Matplotlib (Hunter 2007), a comprehensive library for creating static, animated and interactive visualizations in Python; Astropy (Price-Whelan et al. 2018), a community python library for astronomy.

REFERENCES

- Abadi, M. G., Moore, B., & Bower, R. G. 1999, MNRAS, 308, 947
 Abazajian, K. N., Adelman-McCarthy, J. K., Agüeros, M. A., et al. 2009, ApJS, 182, 543
 Bahé, Y. M., & McCarthy, I. G. 2015, MNRAS, 447, 969
 Baldry, I. K., Balogh, M. L., Bower, R. G., et al. 2006, MNRAS, 373, 469
 Balogh, M. L., Navarro, J. F., & Morris, S. L. 2000, ApJ, 540, 113
 Bell, E. F., McIntosh, D. H., Katz, N., & Weinberg, M. D. 2003, ApJS, 149, 289
 Bell, E. F., Wolf, C., Meisenheimer, K., et al. 2004, ApJ, 608, 752
 Blanton, M. R., & Roweis, S. 2007, AJ, 133, 734
 Blanton, M. R., Schlegel, D. J., Strauss, M. A., et al. 2005, AJ, 129, 2562
 Bluck, A. F. L., Mendel, J. T., Ellison, S. L., et al. 2014, MNRAS, 441, 599
 —. 2016, MNRAS, 462, 2559
 Brinchmann, J., Charlot, S., White, S. D. M., et al. 2004, MNRAS, 351, 1151
 Croton, D. J., Springel, V., White, S. D. M., et al. 2006, MNRAS, 365, 11
 Davies, L. J. M., Robotham, A. S. G., Lagos, C. d. P., et al. 2019, MNRAS, 483, 5444

- Di Matteo, T., Springel, V., & Hernquist, L. 2005, *Nature*, 433, 604
- Gunn, J. E., & Gott, III, J. R. 1972, *ApJ*, 176, 1
- Heckman, T. M., & Best, P. N. 2014, *ARA&A*, 52, 589
- Hirschmann, M., De Lucia, G., Wilman, D., et al. 2014, *MNRAS*, 444, 2938
- Hunter, J. D. 2007, *Computing in Science & Engineering*, 9, 90
- Ilbert, O., McCracken, H. J., Le Fèvre, O., et al. 2013, *A&A*, 556, A55
- Jones, E., Oliphant, T., Peterson, P., et al. 2001–, *SciPy: Open source scientific tools for Python*
- Knobel, C., Lilly, S. J., Woo, J., & Kovač, K. 2015, *ApJ*, 800, 24
- Kroupa, P., & Weidner, C. 2003, *ApJ*, 598, 1076
- Larson, R. B., Tinsley, B. M., & Caldwell, C. N. 1980, *ApJ*, 237, 692
- Lilly, S. J., & Carollo, C. M. 2016, *ApJ*, 833, 1
- Liu, C., Hao, L., Wang, H., & Yang, X. 2019, *ApJ*, 878, 69
- Martig, M., Bournaud, F., Teyssier, R., & Dekel, A. 2009, *ApJ*, 707, 250
- Mendel, J. T., Simard, L., Palmer, M., Ellison, S. L., & Patton, D. R. 2014, *ApJS*, 210, 3
- Mo, H. J., & Mao, S. 2004, *MNRAS*, 353, 829
- Mo, H. J., Mao, S., & White, S. D. M. 1999, *MNRAS*, 304, 175
- Moore, B., Katz, N., Lake, G., Dressler, A., & Oemler, A. 1996, *Nature*, 379, 613
- Murray, N., Ménard, B., & Thompson, T. A. 2011, *ApJ*, 735, 66
- Peng, Y.-j., Lilly, S. J., Kovač, K., et al. 2010, *ApJ*, 721, 193
- Price-Whelan, A. M., Sipőcz, B. M., Günther, H. M., et al. 2018, *AJ*, 156, 123
- Read, J. I., Wilkinson, M. I., Evans, N. W., Gilmore, G., & Kleya, J. T. 2006, *MNRAS*, 366, 429
- Shi, J., Wang, H., Mo, H., et al. 2020, *arXiv e-prints*, arXiv:2001.04090
- Simard, L., Mendel, J. T., Patton, D. R., Ellison, S. L., & McConnachie, A. W. 2011, *ApJS*, 196, 11
- Strateva, I., Ivezić, Ž., Knapp, G. R., et al. 2001, *AJ*, 122, 1861
- Teimoorinia, H., Bluck, A. F. L., & Ellison, S. L. 2016, *MNRAS*, 457, 2086
- Tomczak, A. R., Quadri, R. F., Tran, K.-V. H., et al. 2014, *ApJ*, 783, 85
- Toomre, A., & Toomre, J. 1972, *ApJ*, 178, 623
- van den Bosch, F. C., Aquino, D., Yang, X., et al. 2008, *MNRAS*, 387, 79
- van der Walt, S., Colbert, S. C., & Varoquaux, G. 2011, *Computing in Science Engineering*, 13, 22
- van der Wel, A., Franx, M., van Dokkum, P. G., et al. 2014, *ApJ*, 788, 28
- Wang, E., Wang, H., Mo, H., van den Bosch, F. C., & Yang, X. 2020, *ApJ*, 889, 37
- Wang, E., Wang, H., Mo, H., et al. 2018a, *ApJ*, 860, 102
- Wang, H., Mo, H. J., Chen, S., et al. 2018b, *ApJ*, 852, 31
- Weinmann, S. M., van den Bosch, F. C., Yang, X., & Mo, H. J. 2006, *MNRAS*, 366, 2
- Wetzell, A. R., Tinker, J. L., & Conroy, C. 2012, *MNRAS*, 424, 232
- White, S. D. M., & Rees, M. J. 1978, *MNRAS*, 183, 341
- Woo, J., Dekel, A., Faber, S. M., et al. 2013, *MNRAS*, 428, 3306
- Yang, X., Mo, H. J., & van den Bosch, F. C. 2009, *ApJ*, 695, 900
- Yang, X., Mo, H. J., van den Bosch, F. C., et al. 2007, *ApJ*, 671, 153